Commensal myeloid crosstalk in neonatal skin regulates long-term cutaneous type 17 inflammation

Miqdad O. Dhariwala[1], Andrea M. DeRogatis[1], Joy N. Okoro[1,2], Antonin Weckel[1], Victoria M. Tran[1,2], Irek Habrylo[1,2], Oluwasunmisola T. Ojewumi[1%], Allison E. Tammen[1†], John M. Leech[1‡], Geil R. Merana[1,2§], Ricardo O. Carale[1], Rio Barrere-Cain[1], Kamir J. Hiam-Galvez[2,3¶], Matthew H. Spitzer[3], and Tiffany C. Scharschmidt[1]

Affiliations:

[1] Department of Dermatology, University of California San Francisco; San Francisco, CA USA

[2] Biomedical Sciences Program, University of California San Francisco; San Francisco, CA USA

[3] Department of Otolaryngology-Head and Neck Surgery, Department of Microbiology and Immunology, Parker Institute for Cancer Immunotherapy, University of California San Francisco; San Francisco, CA USA

[%] Current affiliation: Biomedical Sciences Program, Cornell University; Ithaca, NY USA

[†] Current affiliation: Molecular Microbiology and Immunology, Oregon Health Science University; Portland, OR, USA

[‡] Current affiliation: Pfizer; New York, NY USA

[§] Current affiliation: Genentech; South San Francisco, CA, USA

[¶] Current affiliation: Stanford University; Palo Alto, CA, USA

Lead contact: Tiffany C. Scharschmidt tiffany.scharschmidt@ucsf.edu

Abstract

Early life microbe-immune interactions at barrier surfaces have lasting impacts on the trajectory towards health versus disease. Monocytes, macrophages and dendritic cells are primary sentinels in barrier tissues, yet the salient contributions of commensal-myeloid crosstalk during tissue development remain poorly understood. Here, we identify that commensal microbes facilitate accumulation of a population of monocytes in neonatal skin. Transient postnatal depletion of these monocytes resulted in heightened IL-17A production by skin T cells, which was particularly sustained among $CD4^+$ T cells into adulthood and sufficient to exacerbate inflammatory skin pathologies. Neonatal skin monocytes were enriched in expression of negative regulators of the IL-1 pathway. Functional in vivo experiments confirmed a key role for excessive IL-1R1 signaling in T cells as contributing to the dysregulated type 17 response in neonatal monocyte-depleted mice. Thus, a commensal-driven wave of monocytes into neonatal skin critically facilitates long-term immune homeostasis in this prominent barrier tissue.

Introduction

Symbiotic relationships established between commensal microbes and the immune system help lay the foundation for tissue homeostasis at body barrier sites. Such interactions are especially pivotal in the early life window for defining the longer-term trajectory of health versus disease[1,2,3]. Neonatal exposure to skin commensal bacteria has been shown to critically shape the composition and function of cutaneous lymphocytes[4]. Work by our group and others have demonstrated the importance of early microbial cues in recruiting $CD4^+$ regulatory T cells (Tregs)[5] and Mucosal Associated Invariant T (MAIT) lymphocytes to the neonatal skin[6], cell types which in turn promote enduring commensal-specific immune tolerance and improved wound repair. Comparatively little is known, however, about early life crosstalk between commensal microbes and skin myeloid cells, despite the sentinel role these cells play in sensing microbial cues.

The developing immune system is enriched, by design, in immune regulatory mechanisms to help limit inflammation in response to an onslaught of new antigenic exposures[7,8]. This extends to barrier tissues, where antigen-presenting cells (APCs) have been specifically implicated in promoting tolerance via Treg generation in the perinatal window. For example, arginase-2 producing dendritic cells (DC) in human prenatal tissues[9], RORγt-expressing antigen-presenting cells in neonatal mesenteric lymph nodes[10], and $CD301b^+$ type 2 DCs in neonatal skin[11] have all been shown to facilitate Treg generation, the latter two specifically in response commensal antigens. What additional mechanisms and other myeloid cell types might contribute to the regulatory environment of developing barrier tissues remain undefined.

Monocytes are circulating mononuclear myeloid cells constitutively produced in the bone marrow that, upon entering non-lymphoid tissues such as skin, can further differentiate into

macrophages and subsets of DCs. Monocytes help initiate and tune immune response via multiple mechanisms including phagocytosis, antigen presentation and cytokine secretion[12]. In mice, functionally distinct monocyte subsets are distinguishable via their respective expression of the chemokine receptors CCR2 and CX3CR1. CCR2^{hi} classical monocytes, are generally recognized for their pro-inflammatory contributions towards initiation of immune response following infection or injury, whereas CX3CR1^{hi} non-classical or patrolling monocytes have described contributions in immune surveillance, tissue-repair and anti-tumor immune responses[13–16]. However, many unanswered questions remain about the composition and function of monocytes in developing barrier tissues, including whether they contribute to the immune regulatory environment and if they differ from their adult counterparts or to those in inflamed tissues.

Here, we set out to better define the early life skin myeloid compartment and its relationship to microbial colonization, uncovering that CCR2^{hi}Ly6C^{hi} monocytes are enriched in murine neonatal skin and that commensal microbes play a vital role in their accumulation. We discovered that transient neonatal depletion of these monocytes led to a persistent, dysregulated type 17 inflammatory response among skin T cells. Heightened expression of IL-1 pathway repressors, IL-1Ra and IL-1R2, by neonatal skin monocytes as well as restoration of a homeostatic type 17 response in monocyte-depleted mice via neonatal blockade of IL-1 signaling, identified IL-1 modulation as a key axis for monocyte-mediated immune regulation in neonatal skin. Our study reports a novel regulatory immune role for monocytes in neonatal tissues, by which they help establish a long-term trajectory for tissue immune homeostasis.

Results

Classical monocytes rapidly accumulate in neonatal skin.

To gain a global understanding of the myeloid cell landscape in murine skin during early postnatal development we used Mass Cytometry (CyTOF) to enumerate skin immune cells in wild type (wt) C57BL6 mice during the first month of life (Fig. 1A). We developed a 34 antibody panel heavily focused on myeloid cell markers along with sufficient lymphocyte epitopes to enable basic identification of T cell subsets. Application of this panel to 6, 15 and 30 day-old back skin revealed stark age-dependent differences as demonstrated by principal component analysis on the $CD45^+$ compartment (Fig. 1B, Fig. S1A). Pooled analysis of skin from all three time points identified 26 distinct clusters of immune cells (Fig. 1C, Fig. S1B). Six were identified as lymphocyte subtypes and fifteen were of clear myeloid origin. The remaining five could not be definitively identified based on our antibody panel, but likely included innate lymphoid cells (ILCs)[17]. Multiple clusters were specifically enriched at distinct time points (Fig. 1D-E). Examination of lymphoid populations revealed stable percentages of Dendritic Epidermal T cells (DETCs) between postnatal day 6 and day 30, consistent with their known prenatal skin seeding[18] (Fig. S1C). Likewise, this dataset confirmed our prior flow cytometry studies demonstrating progressive accumulation of regulatory T cells (Tregs) in skin during the first weeks of postnatal life[5,19] (Fig. S1D).

Examination of myeloid cells also revealed age-dependent shifts in relative cluster abundance. Consistent with recent work[11], type 1 classical dendritic cells (cDC1) were somewhat enriched at the immediate postnatal window, in contrast prevalence of their type 2 counterparts (cDC2) increased at later time points (Fig. S1E). While most other myeloid clusters had their peak relative abundance at day 15 or later (Fig. 1D-E), we noted three clusters that were highly enriched at postnatal day 6. We identified the first of these as MHC-II^{lo} macrophages (cluster

12), which were replaced progressively at days 15 and 30 of life by MHC-II^{mid} and MHC-II^{hi} macrophages, consistent with a gradual process of maturation and activation in the tissue[20] (Fig. S1F-G). The second was a small CD11b^{+} MHCII^{neg} population (cluster 10) that was intermediate for CD24 and Ly6C, and hard to definitively classify (Fig. S1H). The third expressed markers consistent with a monocyte identity, i.e. Ly6c^{hi} CD11b^{hi} CD24^{lo} CD64^{lo} MHCII^{neg} (cluster 11) (Figs. 1F, S1B). These monocytes demonstrated a high day 6 abundance (cumulatively ~6% of all CD45^{+} cells), followed by a precipitous drop off in proportion/density by the day 15 time point (Fig. 1G). Characterization of these neonatal skin monocytes by flow cytometry confirmed their high expression of CCR2 and Ly6C, further identifying them as classical monocytes (Fig. S1I).

Classical monocytes are typically considered pro-inflammatory cells studied in the context of tissue infection or injury[12]. Thus, we were intrigued to see them enriched in neonatal skin, which has a pro-tolerogenic immune tone towards commensal microbes and other antigens[1,19]. To further define the timing of skin monocyte seeding, we performed longitudinal enumeration of skin monocytes by flow cytometry from postnatal day 1 to 30 (Fig 1H). Although skin monocytes were present in 1-day old pups, their percentage and number dramatically increased by postnatal day 3 (Fig. 1I-K). Consistent with our CyTOF data, monocyte numbers remained substantially higher at day 6 before tapering off at later timepoints, likely reflecting their known propensity to downregulate Ly6C and gain MHC-II expression as part of their differentiation into monocyte-derived dendritic cells (Mo-DCs)[21]. In contrast, there were no substantial age-dependent differences in the proportion of monocytes in the spleen over this period (Fig. S1J). Cumulatively, these data demonstrate that the myeloid immune landscape in the skin changes with age and that a population of classical monocytes (neoMono) accumulate in high density and proportion in the early life window.

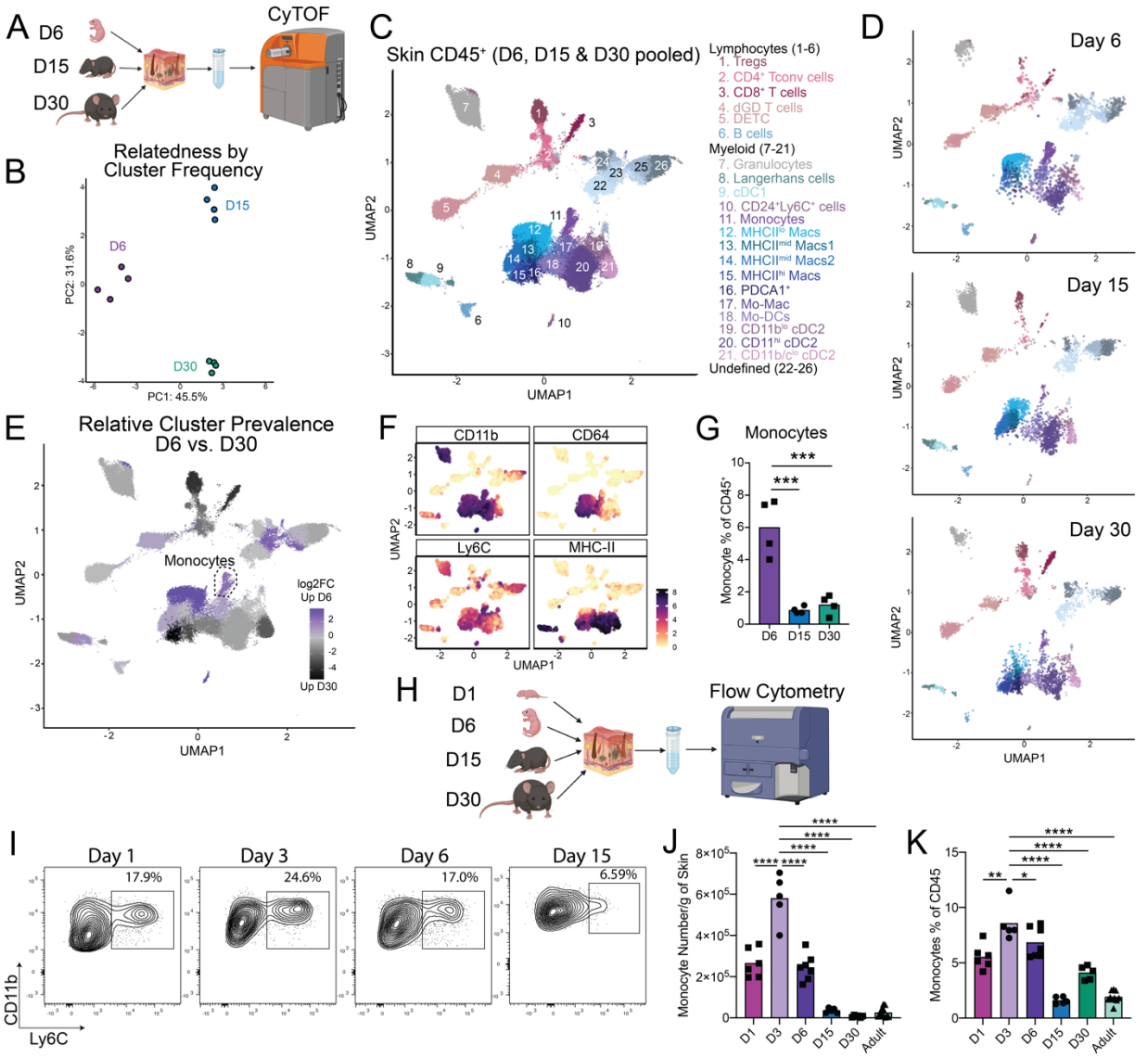

Figure 1: Classical monocytes rapidly accumulate in neonatal skin (A) Skin tissue from mice at the postnatal Day 6, Day 15 and Day 30 ages was harvested and analyzed by Mass Cytometry (CyTOF). (B) Principal component analysis (PCA) plot demonstrating the distribution of the cutaneous $CD45^+$ cellular compartment based on cluster frequency. Each dot represents a single mouse at the indicated age. (C) Pooled UMAP plot demonstrating clusters of $CD45^+$ immune cells in the skin of mice at Day 6, 15 and 30. (D) Individual UMAPs demonstrating immune cell clusters in the skin of Day 6, 15 and 30 mice. (E) UMAP demonstrating clusters of immune cells enriched in the skin of Day 6 (purple) or Day 30 (black) mice. (F) UMAPs demonstrating expression profile of indicated markers to identify monocyte cluster. (G) Enumeration of monocytes as a percent of the total immune cell compartment of the skin at the indicated time points. (H) Back skin from mice at postnatal day 1, 3, 6, 15 & 30 and >8-week-old adult mice was analyzed by Flow Cytometry. (I) Representative flow cytometry plots of skin monocytes at the indicated ages. (J-K) Enumeration of skin monocytes by flow cytometry as (J) total numbers per gram of skin and (K) percentage of $CD45^+$ cells. For CyTOF experiment n=4 mice were used at each time point, for flow cytometry assays >4 mice were used at each time point. Data presented in I-K is one representative of at least two independent experiments. Statistical significance was determined by a One-Way ANOVA where *** is $p<0.001$ and **** is $p<0.0001$.

Commensal microbes facilitate early skin accumulation of monocytes.

Given the postnatal timing of neoMono accumulation in skin, we hypothesized that recognition of microbial ligands might provide the signals necessary to drive their recruitment. To examine this, we performed flow cytometry on skin from day 6 germ-free (GF) and specific-pathogen-free (SPF) pups, which revealed significantly higher neoMono numbers and percentages in the back

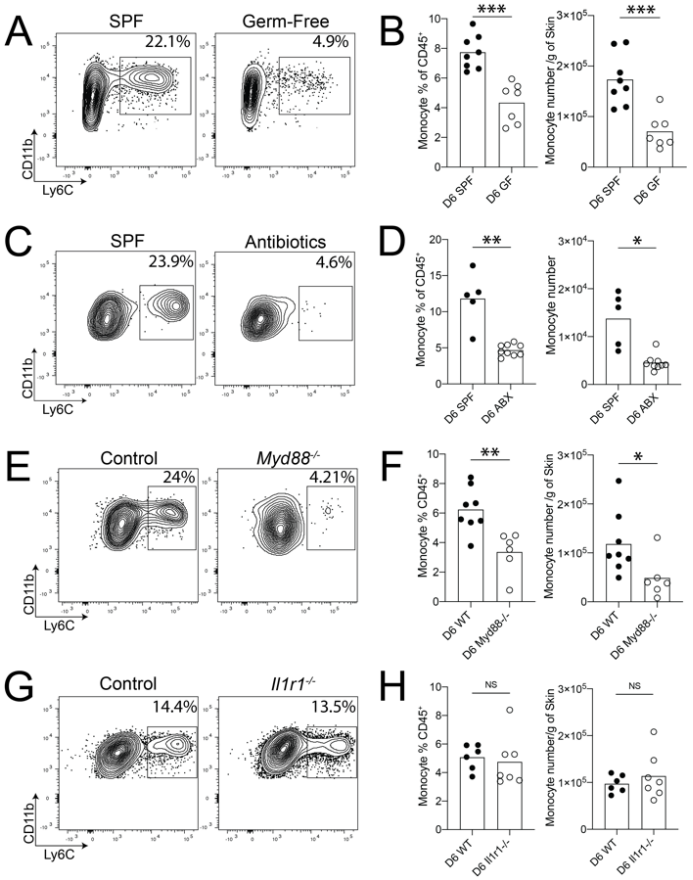

Figure 2: Commensal microbiota facilitate early skin accumulation of monocytes Neonatal skin from mice at the postnatal Day 6 age was harvested and analyzed for monocytes using flow cytometry. Representative flow cytometry plots and quantification of monocyte numbers from (A-B) Specific Pathogen Free (SPF) control and Germ-Free pups, (C-D) SPF control pups and pups born to antibiotic treated dams in cleaner environments, (E-F) Control and *Myd88*$^{-/-}$ pups, (G-H) Control and *Il1r1*$^{-/-}$ pups. Data from (A-B and E-F) are pooled from two experiments where each point represents a single mouse with a pooled n≥5 mice per group, per condition. Data from (C-D and G-H) are one representative of at least two independent experiments with n≥5 mice per group, per condition. Statistical significance was determined by a two-tailed Student's t test where * is p<0.05, ** is p<0.01 and *** is p<0.001

skin of SPF pups as compared to GF pups (Fig. 2A-B). To further assess the requirement for commensal colonization in neoMono skin accumulation we subjected pregnant SPF dams to a cocktail of antibiotics in the drinking water along with frequent cage changes to minimize the microbial load in the bedding. Pups born in these "reduced microbial burden" cages had significantly lower percentages and numbers of skin neoMono on postnatal day 6 (Fig. 2C-D).

Recognizing that commensal microbes can tune levels of alarmin signaling in barrier tissues and that this might serve as a signal for cell recruitment, we next assessed neoMono numbers in the back skin of mice lacking either Myeloid differentiation primary response 88 (*Myd88*$^{-/-}$) or interleukin-1 receptor 1 (*Il1r1*$^{-/-}$). At postnatal day 6, *Myd88*$^{-/-}$ (Fig. 2E-F) but not *Il1r1*$^{-/-}$ (Fig. 2G-H) mice demonstrated significantly lower numbers of skin monocytes. Taken together these data indicate that neoMono skin accumulation is dependent on Myd88 but not IL-1R1 signaling, suggesting that toll-like receptor detection of microbial ligands upstream may be involved.

Neonatal monocyte depletion via anti-Gr1 antibody affects type 17 signature of skin T cells.

To uncover the biological significance of neoMono skin accumulation, we developed a temporal antibody-mediated depletion strategy in the first two weeks of life. By delivering the anti-Gr-1 antibody, which targets cells expressing Ly6G or Ly6C, intraperitoneally to neonatal mice every other day between day 4 and 14 of life, we achieved substantial depletion of skin neoMono as confirmed by flow cytometry on postnatal day 15 (Fig. 3A-C). To gain a broader understanding of the impact of neoMono depletion on the composition and function of the cutaneous immune compartment, we performed single cell RNA-sequencing (scRNA-seq) on CD45^{+} cells sorted from the back skin of anti-Gr-1-treated (NeoΔMono) versus isotype-treated (Control) mice on postnatal day 15 (Fig. 3A). Our analysis showed 20 clearly distinguishable clusters (Fig. 3D) which, based on their expression of key markers (Fig. S2A-B) could be primarily categorized as lymphoid cells or myeloid cells with the exception of one cluster defined primarily by their proliferative status and a small number of contaminating keratinocytes (KC) (Fig. 3E). Examination of relative cluster abundance (Fig. S2C-E) did show a substantial relative reduction in skin monocytes in NeoΔMono versus control skin. Confirmatory flow cytometry studies confirmed anti-Gr-1 depletion of a small population of skin neutrophils, as anticipated based on

their Ly6G expression (Fig. S2F). Other myeloid cell populations such as dendritic cells and macrophages were not significantly affected by neonatal anti-Gr-1 treatment at this time point (Fig. S2G-H).

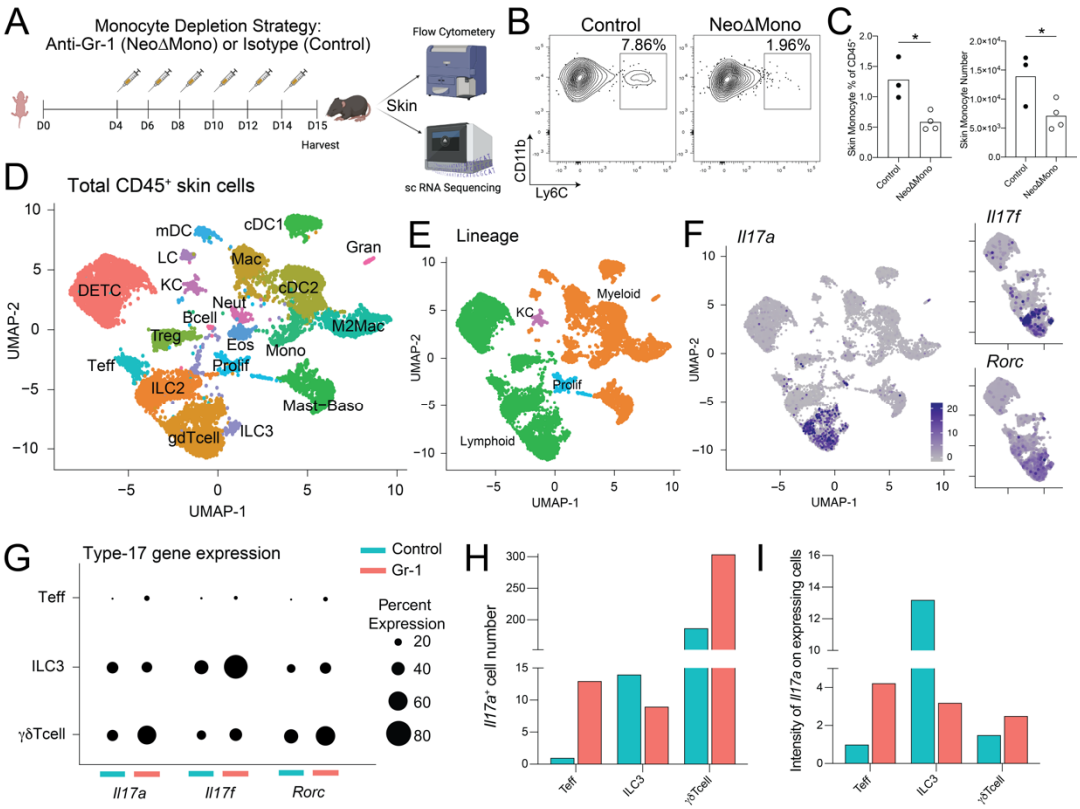

Figure 3: Neonatal monocyte depletion affects type 17 signature of skin T cells (A) Monocytes were depleted in neonatal mice by treatment with the anti-Gr-1 antibody (NeoΔMono mice) and controls were treated with isotype antibody. Skin from these mice was then processed either for flow cytometry or single cell RNA sequencing (scRNA-seq). (B-C) Representative flow plots and quantification of monocytes from the skin of NeoΔMono mice and controls at postnatal Day 15. (D-E) UMAP from scRNA-seq analyses demonstrating clusters of immune cell populations in the skin of NeoΔMono and control mice. (F) UMAPs demonstrating expression profiles of *Il17a*, *Il17f* and *Rorc* in skin lymphoid clusters of NeoΔMono and control mice. (G) Dot plot demonstrating the percent of cells within the cutaneous Teff, ILC3 and γδ T cell clusters that express *Il17a*, *Il17f* and *Rorc* in NeoΔMono and control mice. (H-I) Quantification of the number of *Il17a* expressing cells and intensity of *Il17a* expression in Teff, ILC3 and γδ T cell clusters. For C, statistical significance was determined by a two-tailed Student's t test where * is $p<0.05$. All scRNA-seq analyses were performed post normalizing clusters across both treatment groups.

Our sequencing and flow cytometry data did not reveal substantial differences in the relative proportion or number of effector (i.e. Foxp3^{neg}) CD4^{+} T cells (Teff), Tregs, or γδ T cells in

postnatal day15 NeoΔMono versus control skin (Figs. S2E and S2I). However, further examination of transcripts revealed a shift towards a heightened type 17 signature among $CD4^+$ Teff and dermal γδ T cells, as evidenced by an increased percentage of cells in each cluster expressing *Il17a, Il17f* or *Rorc* (Fig. 3F-G). For *Il17a*, in particular, the total number of *Il17a*-expressing Teff and γδ T cells and the intensity of *Il17a* expression on these cells was increased in NeoΔMono mice (Fig. 3H-I). In contrast, type 3 innate lymphoid cells (ILC3) in NeoΔMono mice showed an overall reduced percentage and intensity of *Il17a* expression (Fig. 3H-I). These data suggest a possible regulatory effect of neoMono on lymphocyte production of the key barrier cytokine IL-17.

Transient early life monocyte depletion leads to sustained enrichment of IL-17A producing skin $CD4^+$ T cells.

To further explore this shift in skin lymphocyte IL-17A production following early life anti-Gr-1 treatment, we performed flow cytometry experiments on NeoΔMono or isotype antibody-treated mice (Fig 4A). Examination of the back skin on day 21 confirmed an increase in the percentage and number of IL-17A producing $CD4^+$ Teff (Figs. 4B and S3A) and dermal γδ T cells (Figs. 4C and S3A). This was also reflected in the corresponding SDLN populations (Fig. 4D-E). As we have previously shown the importance of neonatal skin Tregs in helping to establish tissue immune homeostasis, we examined the skin $CD4^+$ compartment in anti-Gr-1 treated mice which did not reveal significant differences in either the percentage or number of skin Tregs (Fig. 4F) or Teffs (Fig. 4G).

To understand timing of this observed type 17 immune shift, we performed flow cytometry on analogously treated mice on day 15, just after anti-Gr-1 treatment was completed, and 3.5

weeks later on day 40 of life. The day 15 data paralleled our scRNA-seq dataset from the same timepoint showing increases in IL-17A$^+$ skin Teff and dermal γδ T cells (Fig. S3B-C). By day 40, however, it was only the increased skin IL-17A$^+$ skin Teff (Th17) phenotype that persisted in NeoΔMono mice, whereas IL-17A production by dermal γδ T cell had normalized (Fig. S3B-C).

To further verify that the type 17 phenotype was in fact due to the absence of neoMono, we performed analogous experiments delivering an anti-Ccr2 antibody between postnatal day 4 and 14. This alternative monocyte-targeting approach also led to an increase in the percentage and number of skin Th17 cells on postnatal day 21 (Fig. 4H, S3D). As anti-Gr-1 also depletes neutrophils, we performed neonatal delivery of anti-Ly6G antibody to specifically target neutrophils but not monocytes, which did not recapitulate the increased type 17 phenotype (Fig. 4I, S3E). To ascertain if the type 17 phenotype was specific to the anti-Gr-1 treatment in neonatal life or an age independent effect, we performed the anti-Gr-1 treatment in adult mice (Fig. S3F). This did not reveal any significant shifts in IL-17A production by either skin CD4$^+$ Teff (Fig. S3G) or dermal γδ T cells (Fig. S3H), indicating this response is specific to targeting of monocytes in the early life window. Collectively these data suggest that specifically eliminating the observed early life accumulation of neoMono leads to an increase in IL-17A production by skin T cells.

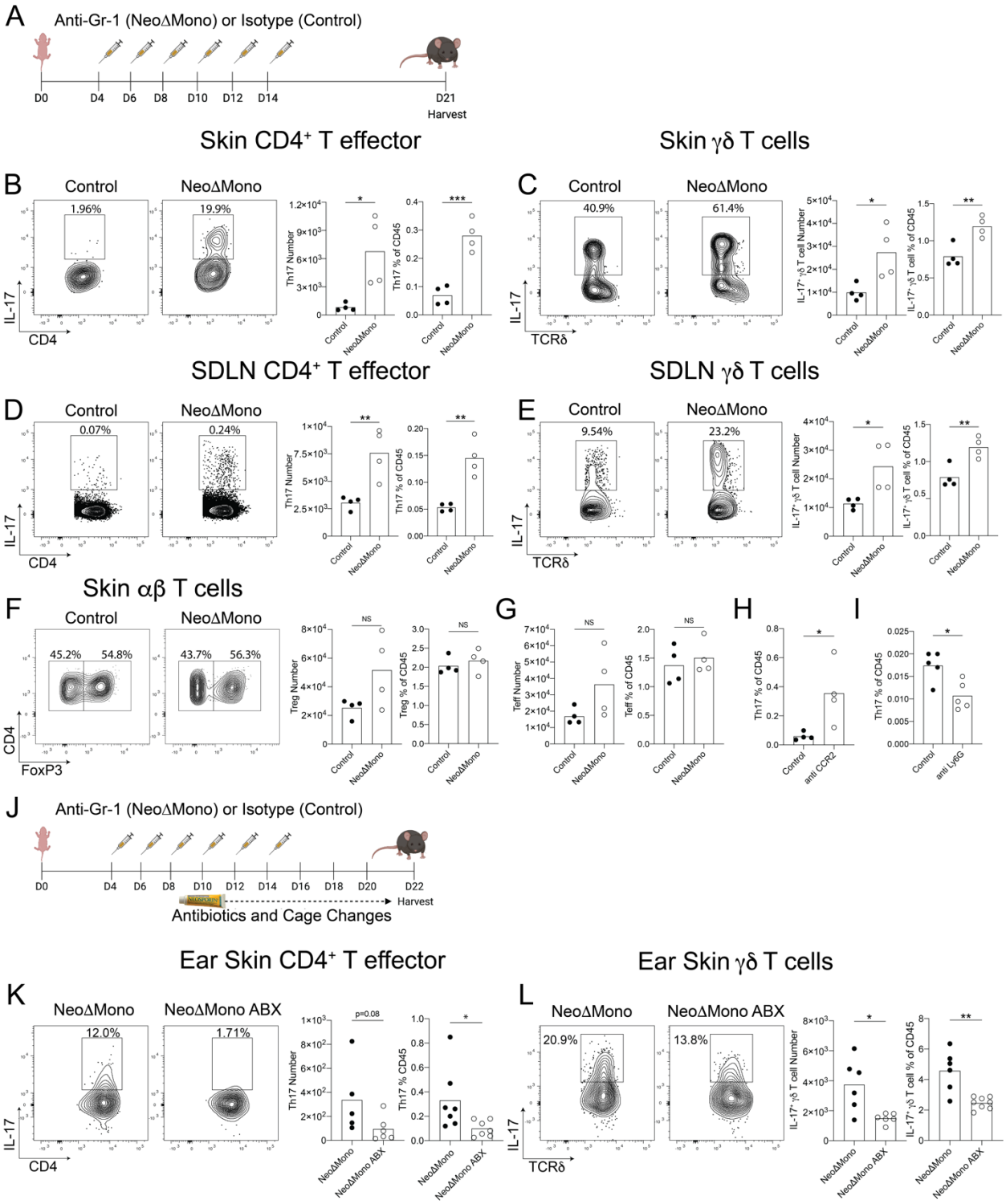

Figure 4: Transient depletion of monocytes in early life leads to sustained type 17 inflammatory responses from cutaneous T lymphocytes. (A) Monocytes were depleted in neonatal mice by treatment with the anti-Gr-1 antibody (NeoΔMono mice) and controls were treated with isotype antibody. Skin from these mice were then processed for flow cytometry at postnatal Day 21. (B & D) Representative flow cytometry plots and quantification of numbers of CD4^{+} T effector cells producing IL-17 in the skin (B)

and skin draining lymph nodes (D). (C & E) Representative flow cytometry plots and quantification of numbers of γδ T cells producing IL-17 in the skin (C) and skin draining lymph nodes (E). (F-G) Representative flow cytometry plots and quantification of numbers of $CD4^+$ T regulatory (F) and effector (G) cells in the skin. (H-I) Quantification of numbers of $CD4^+$ T effector cells producing IL-17 in the skin of mice treated with anti-CCR2 antibody (H) or anti-Ly6G antibody (I) according to the same schedule as in (A). (J) NeoΔMono mice were treated with topical Neosporin and frequent cage changes or controls were treated with vehicle and subjected to mock cage changes. Skin from these mice were then processed for flow cytometry at postnatal Day 22. (K-L) Representative flow cytometry plots and quantification of numbers of $CD4^+$ T effector cells (K) and γδ T cells (L) producing IL-17 in the ear skin. Data in A-G are one representative of at least three independent experiments, H-I are one representative of at least two independent experiments and in J-L are pooled from two experiments that is representative of at least three independent experiments. Statistical significance was determined by a two-tailed Student's t test where * is $p<0.05$, ** is $p<0.01$ and *** is $p<0.001$

Commensal skin microbes contribute to elevated type 17 T cells in NeoΔMono mice.

A body of work has established that the presence of commensal bacteria augments IL-17 producing T cells in skin[22,23]. We thus hypothesized that the increased type 17 response in NeoΔMono might represent a dysregulated response to these commensal microbes. To test this, we performed early life anti-Gr-1 treatment in tandem with an established protocol to deplete skin bacteria[24,25], namely topical application of Neosporin to the ears plus frequent cage changes (Fig. 4J). Examination of skin T cells by flow cytometry on day 22 showed a reduction in the percentage and number of IL-17A producing skin $CD4^+$ Teff (Fig. 4K) and dermal γδ T cells (Fig. 4L), indicating that the presence of neoMono helps to control the homeostatic immune response to skin bacteria.

NeoΔMono mice demonstrate a heightened inflammatory response to imiquimod-driven psoriasiform inflammation.

To elucidate the physiological impact of the dysregulated type 17 inflammatory response in anti-Gr-1 treated NeoΔMono mice, we utilized a well-established murine model of IL-17 driven psoriasiform skin inflammation. Ear skin of 4 week-old NeoΔMono and control mice were treated topically every day for 5 days with 5% imiquimod cream (Fig. 5A). Ear thickness was measured

daily using digital calipers as an indicator of gross inflammation and ear skin and draining lymph nodes were harvested at day 6 for flow cytometric analyses. NeoΔMono mice demonstrated greater ear swelling as early as day 3 of treatment, which became even more substantial by day 5 (Fig. 5B). This ear swelling was accompanied by increased histologic markers of skin inflammation, including a thickened stratum corneum with dysregulated corneocyte differentiation (parakeratosis), accentuated hair follicle plugging and a substantial inflammatory infiltrate in the dermis and subcutis (Fig. 5C-D). Enumeration by flow cytometry (Fig. S4A) revealed a significantly higher neutrophil percentage in the ears (Fig. 5E) and ear-draining lymph nodes (Fig. 5G) of NeoΔMono mice. This paralleled an increase in the percentage and number of Th17 cells in NeoΔMono ear skin (Fig. 5F), which was largely recapitulated in the ear-draining lymph nodes (Fig. 5H, S4B-C). Notably, even though inflammation in this model is known to have a strong contribution from IL-17A-producing dermal γδ T cells, we did not note significant differences in their percentages or numbers between groups (Fig. S4B-C), consistent with our observation that spontaneous IL-17A-production by dermal γδ T cells returns to baseline levels by day 40 (Fig. S3C). Taken together these data suggest that neonatal depletion of monocytes can render mice more susceptible to an IL-17 driven psoriasiform skin inflammation in adulthood.

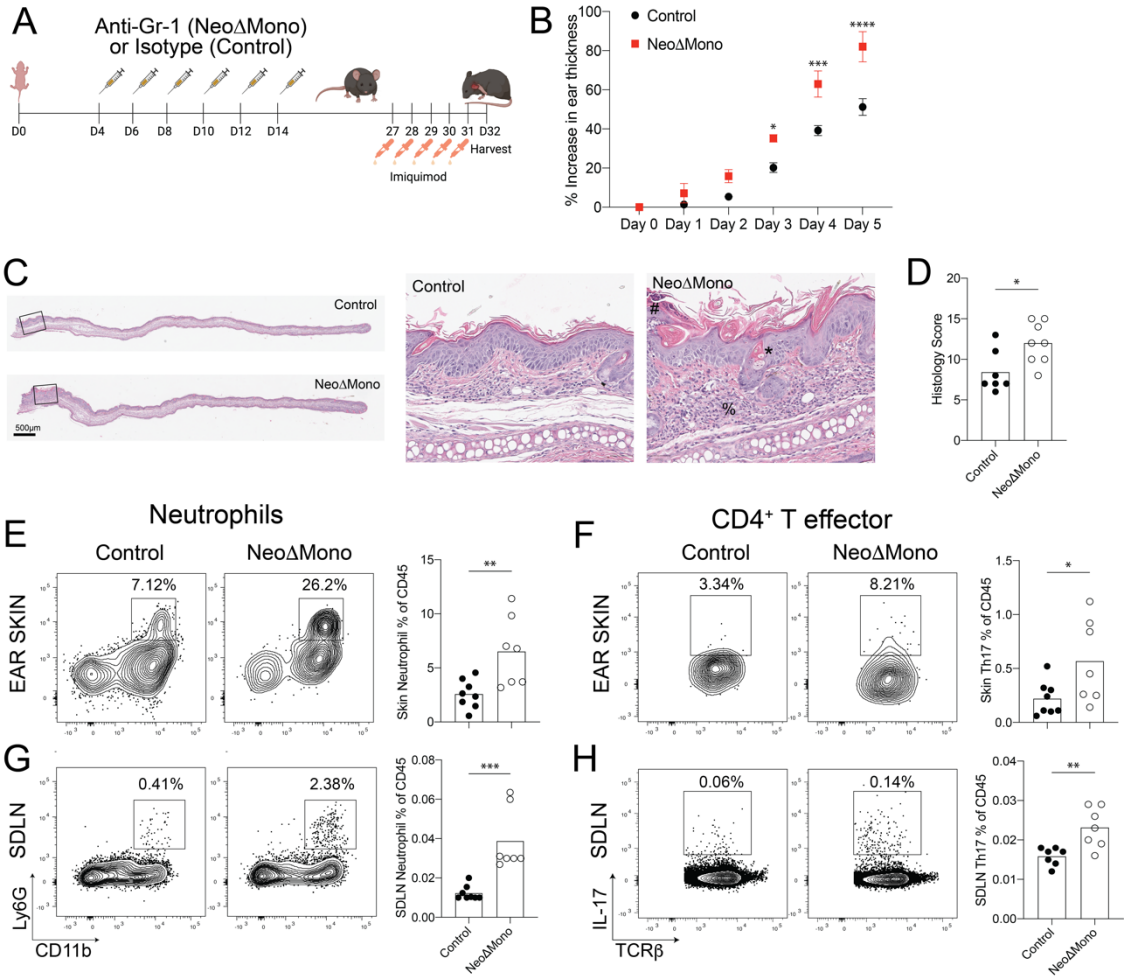

Figure 5: NeoΔmono mice demonstrate a heightened inflammatory response to imiquimod-driven psoriasiform inflammation (A) Monocytes were depleted in neonatal mice by treatment with the anti-Gr-1 antibody (NeoΔMono mice) and controls were treated with isotype antibody. The ears of these mice were treated daily for five days with 5% Imiquimod cream then one day later ear skin and lymph nodes were harvested. (B) Quantification of relative increase in ear thickness as measured with digital calipers during imiquimod treatment in NeoΔMono versus control mice. (C) Representative images of ear skin sections stained with H&E with zoomed inset (C) and quantification of histopathology scoring (D) between groups. # represents parakeratosis (neutrophils in the stratum corneum), * represents hyperkeratosis and plugging and % represents dermal and subcutaneous inflammatory infiltrate. (E-F) Representative flow cytometry plots and quantification of neutrophils (E) and $CD4^+$ Th17 cells (F) in the skin. (G-H) Representative flow cytometry plots and quantification of neutrophils (G) and $CD4^+$ Th17 cells (H) in the skin draining lymph nodes. Data in B is from one of three independent experiments. Data in E-H is data pooled from two independent experiments. Statistical significance in B was determined by a two way ANOVA with Sidak's multiple comparisons test where * is $p<0.05$, *** is $p<0.001$ and **** is $p<0.0001$. Statistical significance in E-H was determined using a two-tailed Student's t test where * is $p<0.05$, ** is $p<0.01$ and *** is $p<0.001$.

Neonatal myeloid cells modulate IL-1 signaling to restrain skin type 17 responses.

We next set out to decipher the mechanism driving the dysregulated type 17 response in the skin of NeoΔMono mice, with a particular focus on $CD4^+$ Teff as the most persistently affected population. To achieve this, we returned to our scRNA sequencing data from D15 control skin to gain further insight into the transcriptional signature of neoMono, and other monocyte-derived skin populations (Fig. 6A). Here we utilized the fast gene set enrichment analysis pipeline in Seurat which revealed an enrichment in IL-1 pathway genes in various myeloid subsets. In particular, the negative regulators of this pathway, namely the IL-1 receptor antagonist IL-1Ra (*Il1rn*) and the decoy receptor IL-1R2 (*Il1r2*), were expressed at very high levels in several myeloid cell types, especially neoMono (Fig. 6B-C, Fig. S5A-B). Further gene set enrichment analysis between specific clusters in this dataset showed neoMono to be particularly enriched for IL-1 pathway genes even when compared to neonatal skin macrophages and the cDC1 subset of dendritic cells (Fig. 6D, S5C). We further examined neoMono expression of IL-1 pathway repressors by performing qPCR for *Il1rn* and *Il1r2* on FACS-sorted monocytes and macrophages from neonatal or adult skin. This confirmed higher *Il1rn* and *Il1r2* transcript levels in neoMono versus neonatal skin macrophages (Fig. 6E, S5D). Additionally, it revealed that this heightened IL-1 pathway repressor expression was particularly enriched among neoMono as compared to analogous monocytes in day 30 skin (Fig. 6E, S5D). These data collectively indicate that skin neoMono are particularly enriched for expression of molecules that make them poised to regulate IL-1 signaling, a pathway known to facilitate IL-17A production by $CD4^+$ lymphocytes[26].

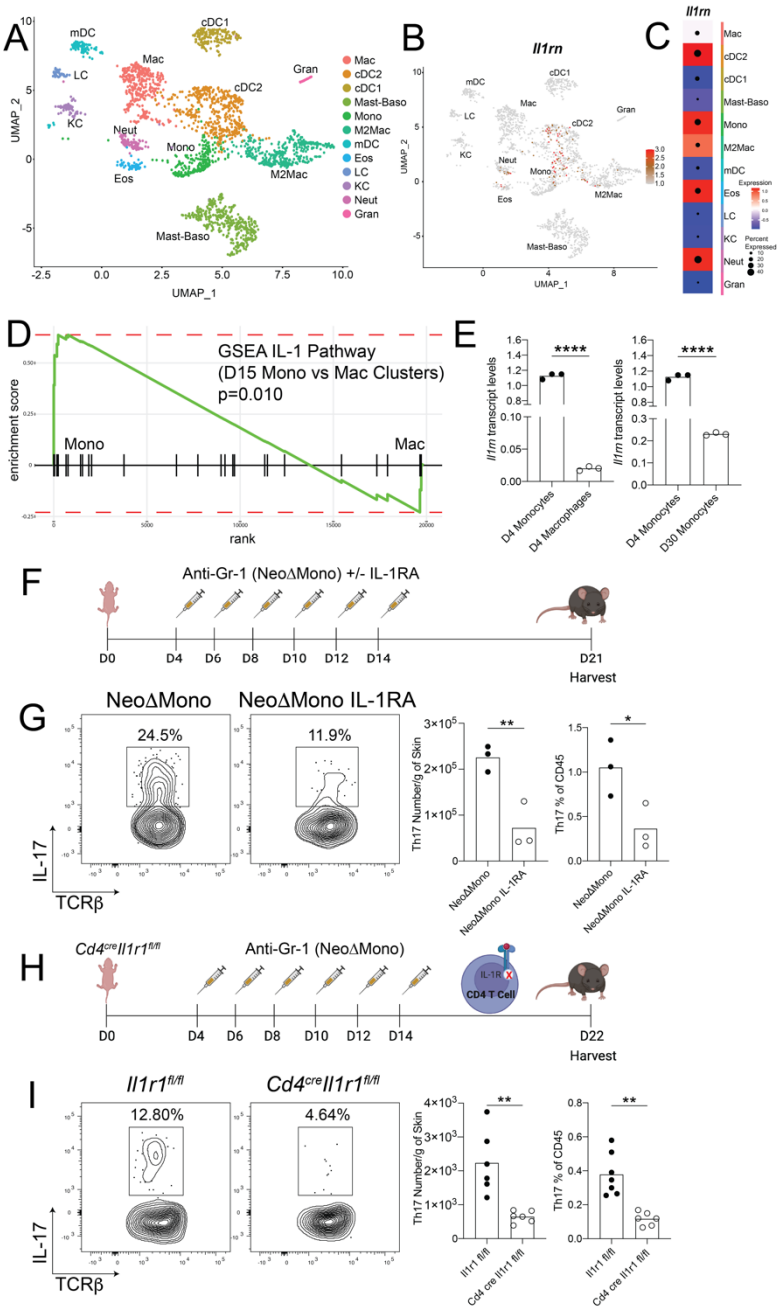

Figure 6: Neonatal monocytes modulate IL-1 signaling to regulate cutaneous type 17 inflammation
(A) UMAP from scRNA-seq analyses demonstrating clusters of myeloid cell populations in the skin of postnatal Day 15 wild type mice. (B) UMAP demonstrating expression levels of *Il1rn* on myeloid clusters. (C) Heatmap quantification of normalized average expression (box color) and percentage of expressing cells (circle size) for *Il1rn* in individual myeloid clusters. (D) Gene Set Enrichment Analyses for IL-1 pathway genes comparing postnatal Day 15 skin monocyte and macrophage clusters. (E) qPCR analyses for *Il1rn* transcript levels comparing monocytes and macrophages from postnatal Day 4 skin and monocytes from postnatal Day 4 skin to monocytes from postnatal Day 30 skin. (F) NeoΔMono mice were either treated with recombinant IL-1Ra or with vehicle. Skin was then processed for flow cytometry on postnatal Day 21. (G) Representative flow cytometry plots and quantification of numbers of $CD4^{+}$ T effector cells producing IL-17A in the skin. (H) Monocytes were depleted in neonatal $Cd4^{cre}Il1r1^{fl/fl}$ or control $Il1r1^{fl/fl}$ mice by treatment with the anti-Gr-1 antibody (NeoΔMono mice). Skin was then processed

for flow cytometry on postnatal Day 21. (I) Representative flow cytometry plots and quantification of numbers of $CD4^+$ T effector cells producing IL-17A in the skin. Statistical significance was determined using a two-tailed Student's t test where * is $p<0.05$, ** is $p<0.01$ and **** is $p<0.0001$. Data in G is representative data from one of three independent experiments and data in I is pooled from two independent experiments.

We thus set out to test the model that depletion of neoMono leads to an increased type 17 immune response via unleashing of IL-1 bioavailability and subsequent signaling. To do so, we treated NeoΔMono mice with low dose recombinant IL-1Ra concurrently with anti-Gr1 administration, in an attempt to compensate for the loss of IL-1 regulation by monocytes (Fig. 6F). Indeed, NeoΔMono mice that received IL-1Ra demonstrated significantly fewer IL-17A producing $CD4^+$ Teff in the skin on day 21 (Fig. 6G). Notably, IL-1Ra treatment between day 4 and 14 was not sufficient to suppress IL-17A production by dermal γδ T cells on day 21 (Fig. S5E), and there was not a statistically significant effect on either $CD4^+$ Teff and dermal γδ T cells in the SDLN (Fig. S5F). To further confirm that heightened IL-1R1 signaling in $CD4^+$ T cells was contributing to their increased propensity for IL-17A production, we crossed *Cd4*^{cre} with *Il1r1*$^{fl/fl}$ mice to achieve deletion of IL-1R1 on $CD4^+$αβ T cells. We then subjected these mice and their *Il1r1*$^{fl/fl}$ littermates to our neonatal regimen of anti-Gr-1 treatment between day 4 and 14 (Fig. 6H). *Cd4*^{cre}*Il1r1*$^{fl/fl}$ mice demonstrated significantly lower percentages and numbers of Th17 cells in the skin on day 21 (Fig. 6I), whereas the effect was again less pronounced in the SDLN (Fig. S5G). Taken together these data suggest that neoMono contribute to negative regulation of IL-1 signaling in the developing tissue, thereby specifically and persistently constraining IL-17 production by skin $CD4^+$ T cells.

Discussion

Here we have identified a prominent postnatal wave of monocytes into skin as a key feature of normal early life development at this prominent body barrier site. Tissue accumulation of these

monocytes early in life is critically facilitated by commensal microbes and requires Myd88-mediated signals. Whereas Ccr2^{hi}Ly6C^{hi}, so called “classical”, monocytes are typically recognized for their role in pro-inflammatory processes, we demonstrate a previously unappreciated regulatory role for them during healthy postnatal development. Depletion of neoMono in this window led to a prolonged increase in IL-17A produced by CD4^{+} $\alpha\beta$ T cells in the skin and draining lymph nodes, with a similar but more transient effect on dermal $\gamma\delta$ T cells. Mechanistically the Th17 response was triggered by augmented upstream IL-1R1 signaling and sustained by the presence of commensal microbiota. Thus, neoMono accumulate in large numbers at the cutaneous interface and, via their enriched expression of IL-1 pathway repressors, help regulate type 17 responses and lower future susceptibility to skin conditions such as psoriasiform inflammation.

Our work demonstrating that commensal microbes facilitate early life skin seeding of CCR2^{hi}Ly6C^{hi} monocytes adds to a growing literature regarding the unique immune composition in developing tissues and the role endogenous microbiota play in shaping this landscape[6,19,27]. Reduced neoMono in *Myd88*$^{-/-}$ but not *Il1r1*$^{-/-}$ skin further suggests that homeostatic TLR activation by commensals in early-life may provide key signals supporting their recruitment. Future studies are needed, however, to further disentangle the individual cell types that provide signals for skin neoMono recruitment as well as the specific chemokines and receptors involved. Given the many skin cell types that express TLRs[28] and the variety of signals that can contribute to monocyte recruitment[29–38], it may be the case that there are multiple and redundant contributors.

Myeloid cells are key initiators of immune responses at barrier sites and as such contribute significantly to setting the immunological tone of these tissues. This has been best described for

DC subsets and other antigen presenting cell types which tune tissue immune function in the skin and gut via their effects on T cells, both augmenting their production of key cytokines[22] and also facilitating immune regulation via generation of Tregs[10,11,39]. In this study we report a previously unappreciated role for neoMono in skin immune regulation. In contrast to DCs, however, this immune regulation does not occur via augmented peripheral Treg generation but rather a direct effect on conventional $CD4^+$ αβ T cells and dermal γδ T cells, namely limiting their production of the important barrier cytokine IL-17A. Depletion of neoMono had a prolonged impact on $CD4^+$ αβ T cells with lasting effects into adulthood, as demonstrated by increased susceptibility of the NeoΔMono mice to psoriasiform inflammation. While the increased IL-17A production was sustained, at least in part, by the presence of skin microbes, it will be important for future studies to disentangle the antigenic specificities and targets of these dysregulated T cell responses.

IL-1 signaling is pivotal in mounting inflammatory responses to eliminate microbial infection and aid in physiological processes such as wound healing[40,41]. Suppression of this pathway by various cell types is critical for resolution of acute inflammatory responses[42,43]. The IL-1 receptor antagonist, or IL-1Ra, along with the decoy receptor IL-1R2 are two key molecules regulating IL-1R1 signaling. Loss of either can influence host susceptibility to infections [44], autoinflammatory disorders[45] and other chronic inflammatory and autoimmune diseases[46,47]. The use of IL-1Ra (Anakinra) in the clinic to treat several skin and systemic disorders[47,48] underscores the importance of the IL-1 pathway and its regulation during inflammation. Comparatively little is known about its functional significance during homeostasis. Previous studies have detected intracellular IL-1Ra in healthy skin[49,50]. Our work highlights that neoMono are specifically enriched in IL-1Ra and IL-R2 expression as compared to other myeloid cell types in skin and also their adult skin counterparts. The factors that elicit expression of these IL-1 pathway

repressors in neoMono and why this is particularly heightened in the postnatal window remain key outstanding questions.

The attenuated Th17 response to neoMono depletion in the setting of IL-1Ra treatment or *Cd4*^{cre}*Il1r1*$^{fl/fl}$ mice indicates that increased tissue availability of IL-1α and/or IL-1β has an effect via direct signaling on CD4^{+} T cells, as opposed to indirect effects via another intermediary population such as DCs. IL-1β has a well-documented role in promoting type 17 responses in T cells[40], especially early in vivo Th17 differentiation via increased *Irf4* and *Rorc* expression[26]. IL-1R1 signaling on memory T cells, however, has also been shown to contribute to heighted production of effector cytokines, including IL-17A, in previously differentiated cells[51]. The fact that we observed a sustained skin Th17 response even into adulthood suggests that altered differentiation and early life fate commitment of naïve CD4^{+} T cells may be the dominant mechanism in our model. In contrast, the effect of neoMono depletion on γδ T cell IL-17A production was fairly transient. While reversal effects in IL-17A production by γδ T cells was not anticipated in *Cd4*^{cre}*Il1r1*$^{fl/fl}$ mice, we were surprised that their cytokine production in NeoΔMono was minimally impacted by IL-1Ra administration. This could be due to innate-like features of γδ T cells, with a lack of committed differentiation. However, we cannot exclude that some pathway other than IL-1R1 signaling is the main mechanism for IL-17A regulation in this cell type[52]. Separately, the lack of an effect for anti-Gr1 treatment in adult life, perhaps explained by the fact that monocytes are comparatively scarce in adult skin and express less IL-1Ra and IL-1R2, suggests that other cell populations might take over the role of IL-1 regulation during adult life. Additionally, the shift towards fewer naïve and more memory CD4^{+} T cells in adult mice might mitigate the impact of increased IL-1R1 signaling on de novo Th17 differentiation.

That the elimination of neoMono leads to unleashing of IL-17A production by skin T cells has important implications for many skin physiological and pathological processes. IL-17A production is critical in skin's ability to fight acute bacterial and fungal infections. Other recent studies have demonstrated additional roles for IL-17 in critical tissue functions such as skin wound healing and nerve regeneration[53,54]. However, when unregulated, it is associated with key pathological processes in skin, namely psoriasis[55,56], hidradenitis suppurativa[56,57], some forms of atopic dermatitis[58] among others[59]. The pleotropic effects of IL-17 suggest a need for tight regulation in the developing tissue to set the foundation for long-term skin health. Our work suggests that even in the absence of tissue inflammation, neonatal monocyte-mediated upstream regulation of IL-1 bioavailability serves as this rheostat for establishing a balanced type 17 lymphocyte compartment.

The idea that monocytes can serve regulatory as well as proinflammatory roles is not unprecedented. In fact, this may be a key feature of "patrolling type" CX3CR1^{hi} CCR2^{low} monocytes in blood vessels. Additionally, Ly6C^{hi} monocytes have been shown to limit inflammation to gut commensal organisms after their recruitment to the site of intestinal infection via production of prostaglandin E2[60]. By comparison, our findings demonstrate a novel regulatory function for these Ly6C^{hi} neoMono in healthy tissue and one that is especially critical and heightened during postnatal life. This work emphasizes the importance of continuing to dissect fundamental mechanisms shaping tissue immunity the early life window as these may uncover new opportunities to understand the long-lasting immune effects that can be imparted by early life exposures and their contribution to human health.

STAR Methods

RESSOURCES AVAILABILITY

Lead contact

Further information and requests for resources and reagents should be directed to and will be fulfilled by the lead contact, Tiffany Scharschmidt (tiffany.scharschmidt@ucsf.edu)

Material availability

All unique/stable reagents generated in this study are available from the Lead Contact with a completed Materials Transfer Agreement.

Data and code availability

Schematics were made with Biorender (https://biorender.com). Rstudio v4 was used for scRNAseq and CyTOF analysis. The scRNA-seq data generated in this study has been deposited into GEO and will be publicly available once this manuscript is accepted for publication.

EXPERIMENTAL MODEL AND SUBJECT DETAILS

Experimental Animals

Wild-type C57BL/6 mice were originally purchased from Jackson Laboratories (Bar Harbor, ME), then bred and maintained in the UCSF specific pathogen-free (SPF) facility on the Parnassus campus for use in experiments. *Cd4*^{cre} and *Il1r1*$^{fl/fl}$ mice were purchased from Jackson Laboratories and bred in-house. *Myd88*$^{-/-}$ and *Il1r1*$^{-/-}$ mice were obtained respectively from the labs of Averil Ma and Clifford Lowell at University of California, San Francisco (UCSF). Gnotobiotic C57BL/6J mice (females and males, at indicated ages) were obtained from the UCSF Gnotobiotics core facility (gnotobiotics.ucsf.edu) and housed in gnotobiotic isolators for the duration of each experiment (Class Biologically Clean).

The age of all experimental animals is indicated in each figure. Littermates of the same sex were socially housed under a 12-hour light/dark cycle and randomly assigned to experimental groups whenever possible. Animal work was performed in accordance with the NIH Guide for the Care and Use of Laboratory Animals and the guidelines of the Laboratory Animal Resource Center and Institutional Animal Care and Use Committee of the University of California, San Francisco.

Methods Details

Antibiotic treatments:

For systemic antibiotic treatment in Figure 2, a cocktail of antibiotics including Ampicillin (1mg/ml), Metronidazole (1mg/ml). Sulfamethoxazole (0.8mg/ml) and Trimethoprim (0.16mg/ml) was dissolved in the drinking water and supplied to pregnant dams. To reduce the microbial burden in the environment, cages were changed every other day for the antibiotic treated mice whereas controls cages were changed once a week as per conventional housing and husbandry policies. Control animals underwent mock cage changes. For topical antibiotic treatments in Figure 4, commercially available Neosporin was applied on the ear skin of mice with cotton swab applicators at the indicated ages and intervals. Control mice were treated with Vaseline.

Antibody injections: Mice were injected with either the anit-Gr-1 (100ug) (Bioxcell, InvivoMAb Catalog No. BE0075), Ly6G (100ug) (Bioxcell, InvivoMAb Catalog No. BE0075-1), Ccr2 (2mg/kg, provided by Matthias Mack and Amar Nijagal) or isotype control (100ug) (Bioxcell, InvivoMAb Catalog No. BE0090) via the intraperitoneal route at the indicated time points.

Mouse skin processing: Back skin was shaved and harvested, lightly defatted, and then minced with scissors to a fine consistency before tissue digestion in 3 mL complete RPMI (RPMI plus 10% fetal calf serum, 1% penicillin-streptomycin, β-mercaptoethanol, glutamate, sodium pyruvate, HEPES and non-essential amino acids) then supplemented with 2 mg/mL collagenase XI, 0.5 mg/mL hyaluronidase, 0.1 mg/mL DNase I (digestion media). Ear pinna skin was split and dorsal and ventral sheets were placed in PBS. Ear skin was then processed similarly to the back skin in a 1ml total volume of digestion media. Digested skin samples were then incubated, with shaking, at 37ºC for 45 minutes before quenching with 10 mL of complete RPMI media and shaking by hand for 30 seconds. Skin cell suspensions were filtered through sterile cell strainers (100 µm followed by 40 µm).

Mouse lymph node processing: Skin draining lymph nodes were harvested and then processed by gentle grinding with a sterile plunger over sterile wire mesh in 1 mL of complete RPMI media to generate a single cell suspension for further analyses.

Cell counting: All tissues were re-suspended in 1 mL PBS and 25 µL of cell suspension was mixed with 25 µL of AccuCheck counting beads (Invitrogen,Catalog No. PCB100) for calculating absolute numbers of cells.

Flow Cytometry

Antibody Staining of Myeloid Populations: Cells were stained in PBS with a Live/Dead marker (Ghost Dye Violet510, Tonbo Biosciences, Catalog No. 13-0870-T100), followed by Fc block (Fisher Scientific, Catalog No. BDB564219) for 15 minutes each at 4ºC. Surface antibodies were added in blocking solution and cells stained for 60 minutes at 4ºC. Cells were then washed and fixed in Paraformaldehyde (PFA) for 30 minutes at 4ºC.

Antibody Staining of Lymphoid Populations: Cells were stained in blocking solution with a Live/Dead marker (Ghost Dye Violet510, Tonbo Biosciences) for 30 minutes at 4ºC. For intracellular staining, cells were fixed and permeabilized using the Foxp3 staining kit (eBioscience, Catalog No. 00-5523-00) buffer for 30 minutes at 4ºC then stained in permeabilization buffer for 30 minutes at 4ºC.

Cell Re-stimulation for Cytokines: After isolation, skin or SDLN single cell suspensions were stimulated with Tonbo kit (1/100 in 1 mL) for 3-6 hours before being processed for staining. A subset of cells was incubated in Brefeldin A to be used as an unstimulated control for gating.

Flow cytometry and analyses: Stained cells were run on a Fortessa (BD Biosciences) in the UCSF Flow Cytometry Core. Flow cytometry data was analyzed using FlowJo software (FlowJo, LLC).

Mass cytometry and analyses: Single cell suspensions were incubated for 1 minute with 25 mM Cisplatin (Sigma-Aldrich, P4394) to allow subsequent cell viability measurement, then fixed in 1.5% paraformaldehyde (Electron Microscopy Sciences) and frozen down in the presence of 10% di- methyl sulfoxide (DMSO) and 10% bovine serum albumin (BSA) at stored at 80ºC for subsequent staining. Individual vials were thawed and $2x10^6$ cells were barcoded using the Cell-ID 20-Plex Pd Barcoding Kit (Fluidigm, product number 201060) for 15 minutes at room temperature. Palladium based barcoding was used as this has been reported to not only enable simultaneous staining of up to 20 different samples but also enable doublet discrimination[61]. All the barcoded samples were then combined into a single tube and cells were stained with metal conjugated antibodies, purchased either from BD Biosciences or Fluidigm. Surface antigens were stained in cell staining media (0.5% BSA, 0.02% Sodium azide in PBS) for 30 minutes at

room temperature with gentle agitation. For intracellular staining, cells were permeabilized using the FOXP3-staining buffer kit (eBioscience) and then incubated for another 30 minutes at room temperature with intracellular antibodies in the presence of the FOXP3-staining kit permeabilization buffer. Cells were stored overnight at 4°C in a buffer containing iridium and then run on a Helios CyTOF system (Fluidigm) in the UCSF, Parnassus flow cytometry core facility.

CyTOF data analysis was performed using the *Cyclone* R package[62]. To identify cell clusters, unsupervised clustering was implemented using the *FlowSOM* algorithm with an optimized 6 by 5 grid to generate 30 clusters[63]. The resulting cell clusters were manually annotated with cell type based on the lineage marker expression profile of each cluster. The markers B220 and NK1.1 demonstrated poor staining quality based upon downstream analysis and were consequently excluded from the unsupervised clustering algorithm. Uniform Manifold Approximation and Projection (UMAP) dimensionality reduction was performed using the *uwot* R package and used to visualize the relationship between cell clusters[64]. To broadly gauge the effect of age, principal-component analysis (PCA) was performed separately on cluster lineage marker expression as well as the percentage of cells per cluster using the prcomp function from the *stats* R package[65].

Single cell RNA sequencing: Live singlet immune cell populations (CD45^{+}) from the back skin of postnatal D15 mice treated with anti-Gr-1 antibody or isotype controls were sorted using a BD FACSAria II with a 100 µm nozzle into RPMI medium supplemented with 10% FBS. Cells were sorted from pooled tissue from 4-7 mice and different conditions were run on separate lanes of a 10X Chromium chip with 3′ v.2 chemistry (10X Genomics) as per the manufacturer's instructions by the UCSF Institute for Human Genetics Sequencing Core. Libraries were

sequenced on an Illumina NovaSeq 6000. FASTQ files were aligned to the mm10 reference genome, and barcode matrices were generated using CellRanger 2.1.

Downstream data analysis, including clustering, visualizations and exploratory analyses, were performed using Seurat 4.0. Cells with <200 features or more than 5000, or >10% mitochondrial genes, and >30% ribosomal genes were filtered out during preprocessing. Principal component analysis (PCA) and uniform manifold approximation and projection (UMAP) were run on the RNA data, and clustering was generated using the first 25 principal components and a resolution of 1. Fast gene set enrichment analyses (fGSEA) for the IL-1 pathway was performed using the genes *Adamts4, Adamts5, App, Casp8, Col3a1, Csf2, Cxcl2, Ifng, Il17a, Il1a, Il1b, Il22, Il6, Mapk8, Mmp13, Mmp14, Mmp3, Mmp8, Mmp9, Nos2, S1008, Sele, Smad6, Tnf, Il1rn, Il1r2.*

Quantitative RT-PCR: Indicated populations were sorted into RLT Plus lysis buffer (Qiagen) and stored at -80°C, then processed using Allprep DNA/RNA micro kit (Qiagen) per manufacturer's protocol. For qPCR analyses, RNA was reverse transcribed using SuperScript III cDNA synthesis kit (ThermoFisher) and amplified using Power SYBR Green PCR master mix (ThermoFisher). *Il1rn* primers: 5′- TAGACATGGTGCCTATTGACCT -3′, forward, and 5′- TCGTGACTATAAGGGGCTCTTC -3′, reverse. *Il1r2* primers: 5′- GATCCAGTCACAAGGGAGGA -3′, forward, and 5′- CCAGGAGAACGTGGAAGAGA -3′, reverse. *Rsp17* gene was used as a housekeeping gene and amplified with the following primers: 5'- ATTGAGGTGGATCCCGACAC -3', forward; 5'- TGCCAACTGTAGGCTGAGTG -3', reverse.

Quantification and statistical analyses: The number of mice per group and independent experimental repeats are annotated in each of the corresponding figure legends. Mice were

allocated randomly into experimental groups after matching for age and littermates were used as controls as best as possible, wherever applicable. Statistical significance was calculated using the GraphPad (Prism) 9.3.1 software and specifics for each experiment are indicated in the corresponding figure legends. Data presented here always demonstrate the statistical mean.

Acknowledgements: We would like to thank Drs. Michael Rosenblum, Ari Molofsky, Clifford Lowell and Abul Abbas for helpful discussions. We thank Drs. Matthias Mack and Amar Nijagal for providing the anti-Ccr2 antibody. We thank Dr. Clifford Lowell and Dr. Clare Abram for providing the *Il1r1*$^{-/-}$ mice and Dr. Averil Ma for providing the *Myd88*$^{-/-}$ mice. We thank Yongmei Hu for mouse husbandry along with Dolores Espiritu and Minerva Espiritu for lab infrastructure. We thank and acknowledge members of the HSW12 community for helpful discussions. We thank Jessie Turnbaugh and the UCSF Gnotobiotics core for experimental help with Germ-free mice. We acknowledge UCSF's PFCC (RRID:SCR_018206) for assistance in flow cytometry and cell sorting, supported by NIH grants P30 DK063720 and 1S10OD021822-01. We acknowledge the UCSF Genomics CoLab in supporting generation of scRNA-seq data. M.O.D. is supported by NIAMS K99AR079554. This work was funded by T.C.S. NIAID DP2AI144968 and NIAMS R01AR080034.

Declaration of Interests: T.C.S is on the scientific advisory board of Concerto Biosciences. M.H.S. is founder, shareholder and board member of Teiko.bio, has received a speaking honorarium from Fluidigm Inc., Kumquat Bio, and Arsenal Bio, has been a paid consultant for Five Prime, Ono, January, Earli, Astellas, and Indaptus, and has received research funding from Roche/Genentech, Pfizer, Valitor, and Bristol Myers Squibb.

Author Contributions: M.O.D. and T.C.S. drafted the manuscript and figures. M.O.D. performed the experiments and analyzed the data. A.M.D., A.W., I.H. and K.J.H. assisted in bioinformatic

data analyses. A.M.D., J.N.O., A.W., V.M.T., O.T.O., A.E.T., J.M.L., G.R.M., R.O.R., and R.B.C. assisted in performing experiments and M.H.S. provided resources and input on experimental design. T.C.S. and M.O.D. oversaw all study design and data analyses. All authors discussed results and commented on the manuscript.

Inclusion and diversity: Multiple authors of this paper self-identify as an underrepresented ethnic minority in their field of research or within their geographical location. Multiple authors of this paper self-identify as a gender minority in their field of research. One or more of the authors of this paper received support from a program designed to increase minority representation in their field of research. While citing references scientifically relevant for this work, we also actively worked to promote gender balance in our reference list.

References

1. Dwyer, L. R. & Scharschmidt, T. C. Early life host-microbe interactions in skin. *Cell Host & Microbe* **30**, 684–695 (2022).
2. Donald, K. & Finlay, B. B. Early-life interactions between the microbiota and immune system: impact on immune system development and atopic disease. *Nat Rev Immunol* 1–14 (2023) doi:10.1038/s41577-023-00874-w.
3. Lubin, J.-B. *et al.* Arresting microbiome development limits immune system maturation and resistance to infection in mice. *Cell Host Microbe* **31**, 554-570.e7 (2023).
4. Dhariwala, M. O. & Scharschmidt, T. C. Baby's skin bacteria: first impressions are long-lasting. *Trends Immunol* **42**, 1088–1099 (2021).
5. Scharschmidt, T. C. *et al.* Commensal Microbes and Hair Follicle Morphogenesis Coordinately Drive Treg Migration into Neonatal Skin. *Cell Host Microbe* **21**, 467-477.e5 (2017).
6. Constantinides, M. G. *et al.* MAIT cells are imprinted by the microbiota in early life and promote tissue repair. *Science* **366**, eaax6624 (2019).
7. Georgountzou, A. & Papadopoulos, N. G. Postnatal Innate Immune Development: From Birth to Adulthood. *Frontiers in Immunology* **8**, (2017).
8. Rackaityte, E. & Halkias, J. Mechanisms of Fetal T Cell Tolerance and Immune Regulation. *Front Immunol* **11**, 588 (2020).
9. McGovern, N. *et al.* Human fetal dendritic cells promote prenatal T-cell immune suppression through arginase-2. *Nature* **546**, 662–666 (2017).

10. Akagbosu, B. *et al.* Novel antigen-presenting cell imparts Treg-dependent tolerance to gut microbiota. *Nature* **610**, 752–760 (2022).
11. Weckel, A. *et al.* Long-term tolerance to skin commensals is established neonatally through a specialized dendritic cell subgroup. *Immunity* **56**, 1239-1254.e7 (2023).
12. Guilliams, M., Mildner, A. & Yona, S. Developmental and Functional Heterogeneity of Monocytes. *Immunity* **49**, 595–613 (2018).
13. Hanna, R. N. *et al.* Patrolling monocytes control tumor metastasis to the lung. *Science* **350**, 985–990 (2015).
14. Michaud, J.-P., Bellavance, M.-A., Préfontaine, P. & Rivest, S. Real-Time In Vivo Imaging Reveals the Ability of Monocytes to Clear Vascular Amyloid Beta. *Cell Reports* **5**, 646–653 (2013).
15. Carlin, L. M. *et al.* Nr4a1-Dependent Ly6Clow Monocytes Monitor Endothelial Cells and Orchestrate Their Disposal. *Cell* **153**, 362–375 (2013).
16. Olingy, C. E. *et al.* Non-classical monocytes are biased progenitors of wound healing macrophages during soft tissue injury. *Sci Rep* **7**, 447 (2017).
17. Meininger, I. *et al.* Tissue-Specific Features of Innate Lymphoid Cells. *Trends Immunol* **41**, 902–917 (2020).
18. Gentek, R. *et al.* Epidermal γδ T cells originate from yolk sac hematopoiesis and clonally self-renew in the adult. *J Exp Med* **215**, 2994–3005 (2018).
19. Scharschmidt, T. C. *et al.* A Wave of Regulatory T Cells into Neonatal Skin Mediates Tolerance to Commensal Microbes. *Immunity* **43**, 1011–1021 (2015).

20. Winterberg, T. *et al.* Distinct phenotypic features of neonatal murine macrophages. *European Journal of Immunology* **45**, 214–224 (2015).
21. Tamoutounour, S. *et al.* Origins and functional specialization of macrophages and of conventional and monocyte-derived dendritic cells in mouse skin. *Immunity* **39**, 925–938 (2013).
22. Naik, S. *et al.* Commensal–dendritic-cell interaction specifies a unique protective skin immune signature. *Nature* **520**, 104–108 (2015).
23. Lima-Junior, D. S. *et al.* Endogenous retroviruses promote homeostatic and inflammatory responses to the microbiota. *Cell* **184**, 3794-3811.e19 (2021).
24. Uberoi, A. *et al.* Commensal microbiota regulates skin barrier function and repair via signaling through the aryl hydrocarbon receptor. *Cell Host Microbe* **29**, 1235-1248.e8 (2021).
25. Gonzalez, J. R. *et al.* FLG Deficiency in Mice Alters the Early-Life CD4+ T-Cell Response to Skin Commensal Bacteria. *J Invest Dermatol* **143**, 790-800.e12 (2023).
26. Chung, Y. *et al.* Critical regulation of early Th17 cell differentiation by IL-1 signaling. *Immunity* **30**, 576–587 (2009).
27. Dhariwala, M. O. *et al.* Developing Human Skin Contains Lymphocytes Demonstrating a Memory Signature. *Cell Rep Med* **1**, 100132 (2020).
28. Miller, L. S. & Modlin, R. L. Toll-like receptors in the skin. *Semin Immunopathol* **29**, 15–26 (2007).
29. Tsou, C.-L. *et al.* Critical roles for CCR2 and MCP-3 in monocyte mobilization from bone marrow and recruitment to inflammatory sites. *J Clin Invest* **117**, 902–909 (2007).

30. Jia, T. *et al.* Additive roles for MCP-1 and MCP-3 in CCR2-mediated recruitment of inflammatory monocytes during Listeria monocytogenes infection. *J Immunol* **180**, 6846–6853 (2008).

31. Landsman, L. *et al.* CX3CR1 is required for monocyte homeostasis and atherogenesis by promoting cell survival. *Blood* **113**, 963–972 (2009).

32. Mack, M. *et al.* Expression and characterization of the chemokine receptors CCR2 and CCR5 in mice. *J Immunol* **166**, 4697–4704 (2001).

33. Kaufmann, A., Salentin, R., Gemsa, D. & Sprenger, H. Increase of CCR1 and CCR5 expression and enhanced functional response to MIP-1 alpha during differentiation of human monocytes to macrophages. *J Leukoc Biol* **69**, 248–252 (2001).

34. Charo, I. F. & Ransohoff, R. M. The many roles of chemokines and chemokine receptors in inflammation. *N Engl J Med* **354**, 610–621 (2006).

35. Weber, C. *et al.* Specialized roles of the chemokine receptors CCR1 and CCR5 in the recruitment of monocytes and T(H)1-like/CD45RO(+) T cells. *Blood* **97**, 1144–1146 (2001).

36. Ravindran, R., Rusch, L., Itano, A., Jenkins, M. K. & McSorley, S. J. CCR6-dependent recruitment of blood phagocytes is necessary for rapid CD4 T cell responses to local bacterial infection. *Proc Natl Acad Sci U S A* **104**, 12075–12080 (2007).

37. Qu, C. *et al.* Role of CCR8 and other chemokine pathways in the migration of monocyte-derived dendritic cells to lymph nodes. *J Exp Med* **200**, 1231–1241 (2004).

38. Bernhagen, J. *et al.* MIF is a noncognate ligand of CXC chemokine receptors in inflammatory and atherogenic cell recruitment. *Nat Med* **13**, 587–596 (2007).

39. Kedmi, R. *et al.* A RORγt+ cell instructs gut microbiota-specific Treg cell differentiation. *Nature* **610**, 737–743 (2022).

40. Mantovani, A., Dinarello, C. A., Molgora, M. & Garlanda, C. Interleukin-1 and Related Cytokines in the Regulation of Inflammation and Immunity. *Immunity* **50**, 778–795 (2019).

41. Macleod, T. *et al.* The Immunological Impact of IL-1 Family Cytokines on the Epidermal Barrier. *Frontiers in Immunology* **12**, (2021).

42. Arend, W. P., Malyak, M., Guthridge, C. J. & Gabay, C. INTERLEUKIN-1 RECEPTOR ANTAGONIST: Role in Biology. *Annual Review of Immunology* **16**, 27–55 (1998).

43. Peters, V. A., Joesting, J. J. & Freund, G. G. IL-1 receptor 2 (IL-1R2) and its role in immune regulation. *Brain, Behavior, and Immunity* **32**, 1–8 (2013).

44. Dinarello, C. A. Biologic Basis for Interleukin-1 in Disease. *Blood* **87**, 2095–2147 (1996).

45. Broderick, L. & Hoffman, H. M. IL-1 and autoinflammatory disease: biology, pathogenesis and therapeutic targeting. *Nat Rev Rheumatol* **18**, 448–463 (2022).

46. Migliorini, P., Italiani, P., Pratesi, F., Puxeddu, I. & Boraschi, D. The IL-1 family cytokines and receptors in autoimmune diseases. *Autoimmun Rev* **19**, 102617 (2020).

47. Dinarello, C. A. The IL-1 family of cytokines and receptors in rheumatic diseases. *Nat Rev Rheumatol* **15**, 612–632 (2019).

48. Calabrese, L., Fiocco, Z., Satoh, T. K., Peris, K. & French, L. E. Therapeutic potential of targeting interleukin-1 family cytokines in chronic inflammatory skin diseases*. *British Journal of Dermatology* **186**, 925–941 (2022).

49. Gabay, C., Porter, B., Fantuzzi, G. & Arend, W. P. Mouse IL-1 receptor antagonist isoforms: complementary DNA cloning and protein expression of intracellular isoform and tissue

distribution of secreted and intracellular IL-1 receptor antagonist in vivo. *The Journal of Immunology* **159**, 5905–5913 (1997).

50. Shuck, M. E., Eessalu, T. E., Tracey, D. E. & Bienkowski, M. J. Cloning, heterologous expression and characterization of murine interleukin 1 receptor antagonist protein. *European Journal of Immunology* **21**, 2775–2780 (1991).
51. Jain, A., Song, R., Wakeland, E. K. & Pasare, C. T cell-intrinsic IL-1R signaling licenses effector cytokine production by memory CD4 T cells. *Nat Commun* **9**, 3185 (2018).
52. Shibata, K., Yamada, H., Hara, H., Kishihara, K. & Yoshikai, Y. Resident Vδ1+ γδ T Cells Control Early Infiltration of Neutrophils after Escherichia coli Infection via IL-17 Production1. *The Journal of Immunology* **178**, 4466–4472 (2007).
53. Konieczny, P. *et al.* Interleukin-17 governs hypoxic adaptation of injured epithelium. *Science* **377**, eabg9302 (2022).
54. Enamorado, M. *et al.* Immunity to the microbiota promotes sensory neuron regeneration. *Cell* **186**, 607-620.e17 (2023).
55. Lowes, M. A., Suárez-Fariñas, M. & Krueger, J. G. Immunology of Psoriasis. *Annual Review of Immunology* **32**, 227–255 (2014).
56. Fletcher, J. M., Moran, B., Petrasca, A. & Smith, C. M. IL-17 in inflammatory skin diseases psoriasis and hidradenitis suppurativa. *Clinical & Experimental Immunology* **201**, 121–134 (2020).
57. Schlapbach, C., Hänni, T., Yawalkar, N. & Hunger, R. E. Expression of the IL-23/Th17 pathway in lesions of hidradenitis suppurativa. *Journal of the American Academy of Dermatology* **65**, 790–798 (2011).

58. Brunner, P. M. *et al.* Early-onset pediatric atopic dermatitis is characterized by TH2/TH17/TH22-centered inflammation and lipid alterations. *The Journal of Allergy and Clinical Immunology* **141**, 2094–2106 (2018).

59. Liu, T. *et al.* The IL-23/IL-17 Pathway in Inflammatory Skin Diseases: From Bench to Bedside. *Front Immunol* **11**, 594735 (2020).

60. Grainger, J. R. *et al.* Inflammatory monocytes regulate pathologic responses to commensals during acute gastrointestinal infection. *Nat Med* **19**, 713–721 (2013).

61. Zunder, E. R. *et al.* Palladium-based mass tag cell barcoding with a doublet-filtering scheme and single-cell deconvolution algorithm. *Nat Protoc* **10**, 316–333 (2015).

62. Patel, R. K. *et al.* Cyclone: an accessible pipeline to analyze, evaluate, and optimize multiparametric cytometry data. *Frontiers in Immunology* **14**, (2023).

63. Van Gassen, S. *et al.* FlowSOM: Using self-organizing maps for visualization and interpretation of cytometry data. *Cytometry A* **87**, 636–645 (2015).

64. Melville, J., Lun, A., Djekidel, M. N., Hao, Y. & Eddelbuettel, D. uwot: The Uniform Manifold Approximation and Projection (UMAP) Method for Dimensionality Reduction. (2023).

65. R: The R Project for Statistical Computing. https://www.r-project.org/.

Supplementary Materials

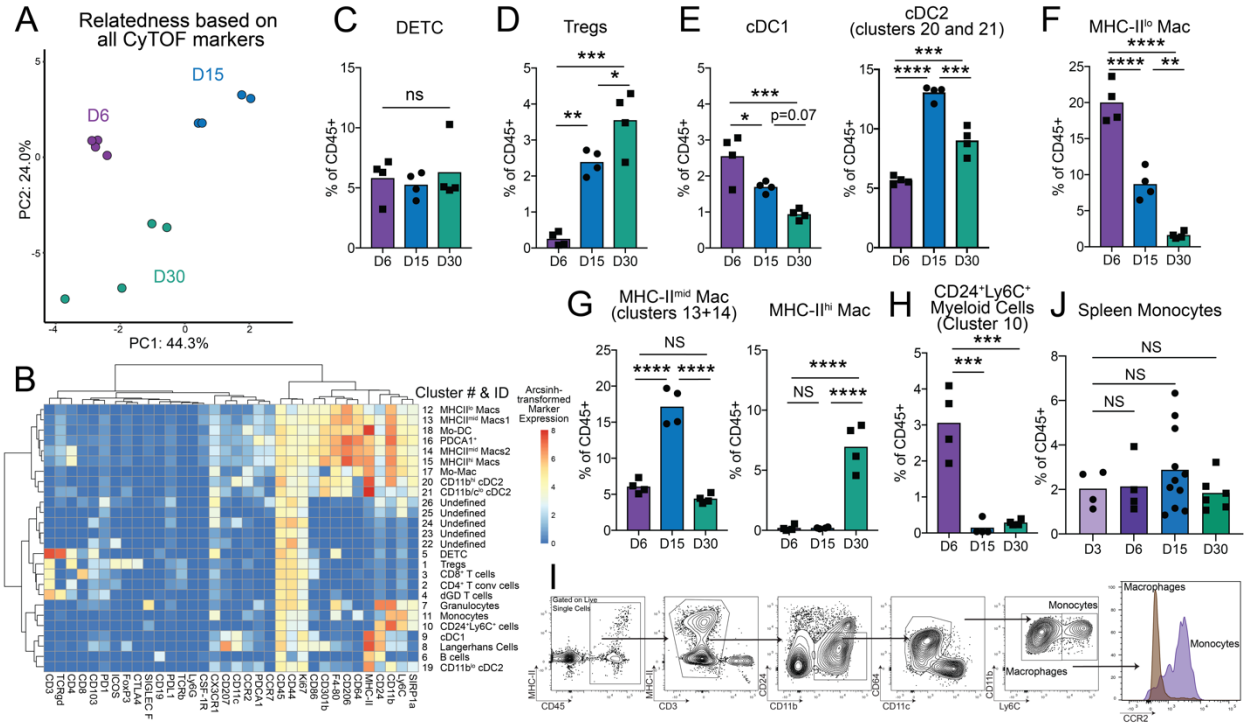

Figure S1: Related to main Figure 1 (A) Principal component analysis (PCA) plot demonstrating the distribution of the cutaneous CD45$^+$ cellular compartment based on marker relatedness. Each dot represents a single mouse at the indicated age. (B) Heat map demonstrating CyTOF marker expression profiles across all immune clusters in postnatal Day 6, Day 15 and Day 30 skin. (C-H) Quantification of Dendritic Epidermal T cells (DETC) (C), Tregs (D), Dendritic Cells (E), Macrophages (F-H) as measured by CyTOF analyses of Day 6, Day 15 and Day 30 skin. (I) Gating strategy used for flow cytometric evaluation of monocytes in murine skin with a histogram demonstrating CCR2 expression levels on cutaneous monocytes and macrophages. (J) Flow cytometric quantification of monocytes in the spleen of postnatal Day 3, 6, 15 and 30 old mice. For CyTOF assays an n=4 mice were used at each time point, for flow cytometry assays an n>4 mice was used at each time point. Statistical significance was determined by a One-Way ANOVA where ** is p<0.01 *** is p<0.001 and **** is p<0.0001.

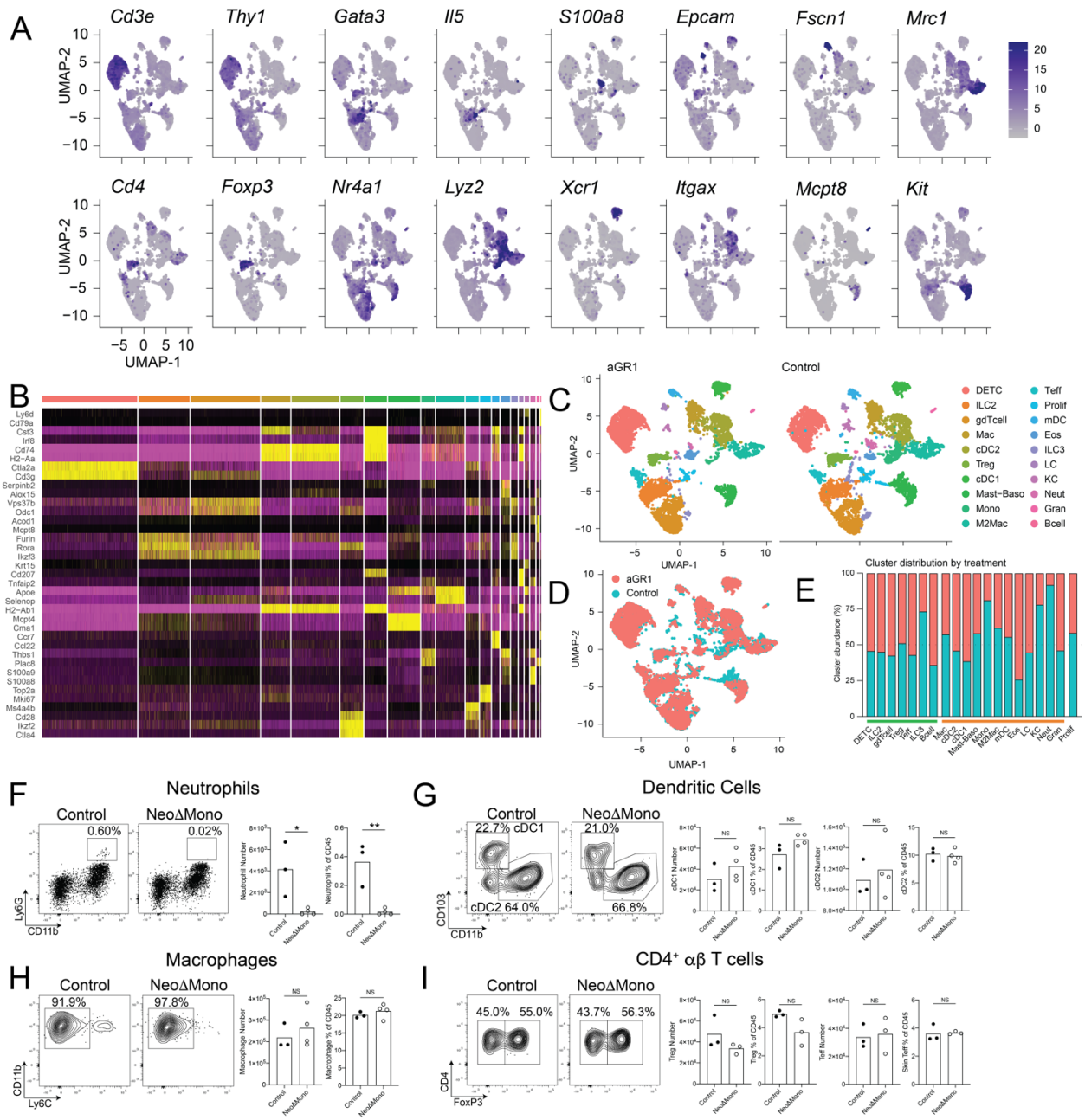

Figure S2: Related to main Figure 3 (A) UMAPs demonstrating expression profiles of indicated genes in skin immune clusters of NeoΔmono and control mice. (B) Heatmap of genes used to define clusters in Fig. 3D. (C-D) Individual and overlaid UMAPs demonstrating immune cell clusters in the skin of anti-Gr-1 treated NeoΔmono and isotype treated control mice. (E) scRNA sequencing based quantification of relative cluster abundance in skin of anti-Gr-1 treated NeoΔmono and isotype treated control mice. (F-I) Representative flow cytometry plots and quantification of neutrophils (F), dendritic Cells (G), macrophages (H) and $CD4^+$ T cells (I) in the skin of NeoΔmono and control mice on postnatal Day 15 of life. All scRNA-seq analyses were performed post normalizing clusters across both treatment groups. In F-I, statistical significance was determined by a two-tailed Student's t test where * is $p<0.05$ and ** is $p<0.01$.

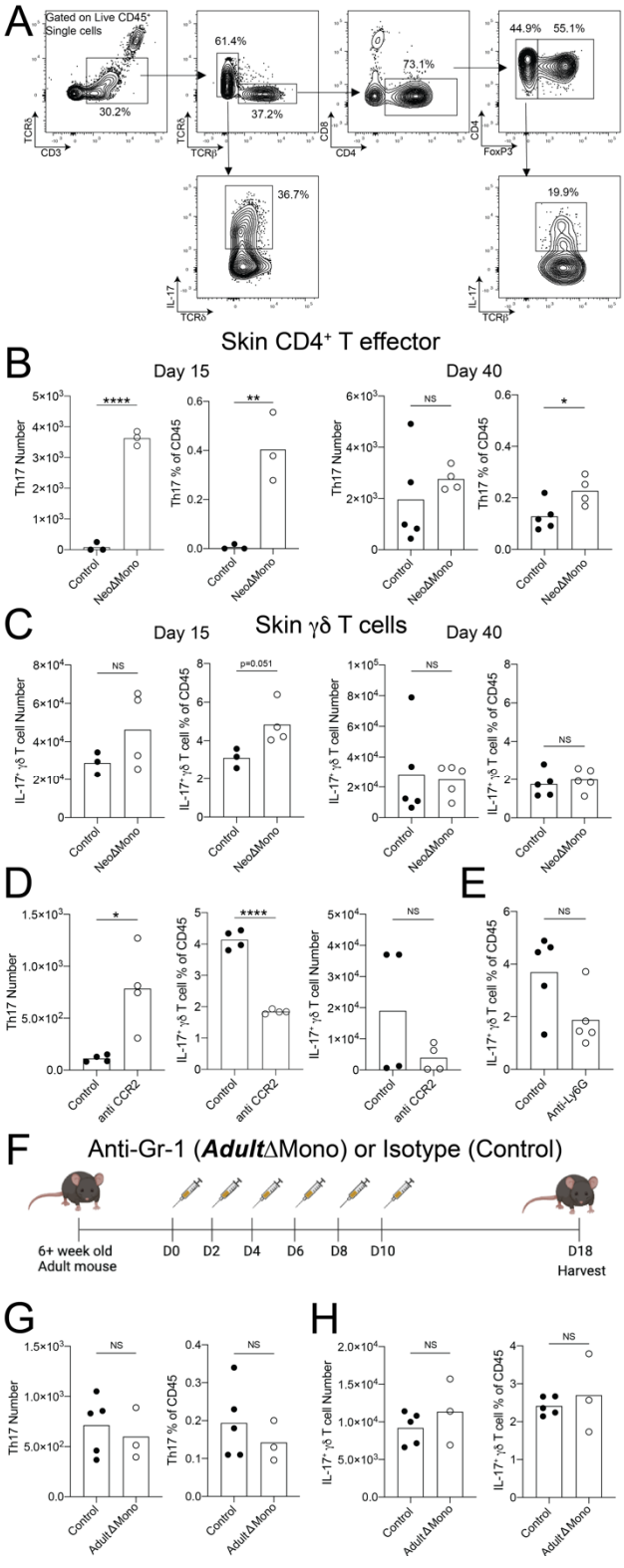

Figure S3: Related to main figure 4 (A) Flow cytometric gating strategy to examine IL-17 producing γδ T cells and $CD4^+$ αβ T effector cells in the skin. (B-C) Quantification of IL-17 producing $CD4^+$ αβ T effector cells (B) and γδ T cells (C) in the skin of NeoΔmono and control mice at postnatal Day 15 and Day 40. (D-E) Quantification of numbers of $CD4^+$ T effector cells producing IL-17 in the skin of mice treated with anti-CCR2 antibody (D) or anti-Ly6G antibody (E). (F) Monocytes were depleted in >8week old adult mice by treatment with the anti-Gr-1 antibody (*Adult*Δmono mice) and controls were treated with isotype antibody. Skin from these mice were then processed for flow cytometry at indicated time points. (G-H) Quantification of IL-17A producing $CD4^+$ αβ T effector cells (G) and γδ T cells (H) in the skin of *Adult*Δmono and control mice. Data here are one representative of atleast two independent experiments. Statistical significance was determined by a two-tailed Student's t test where * is $p<0.05$, ** is $p<0.01$ and **** is $p<0.0001$

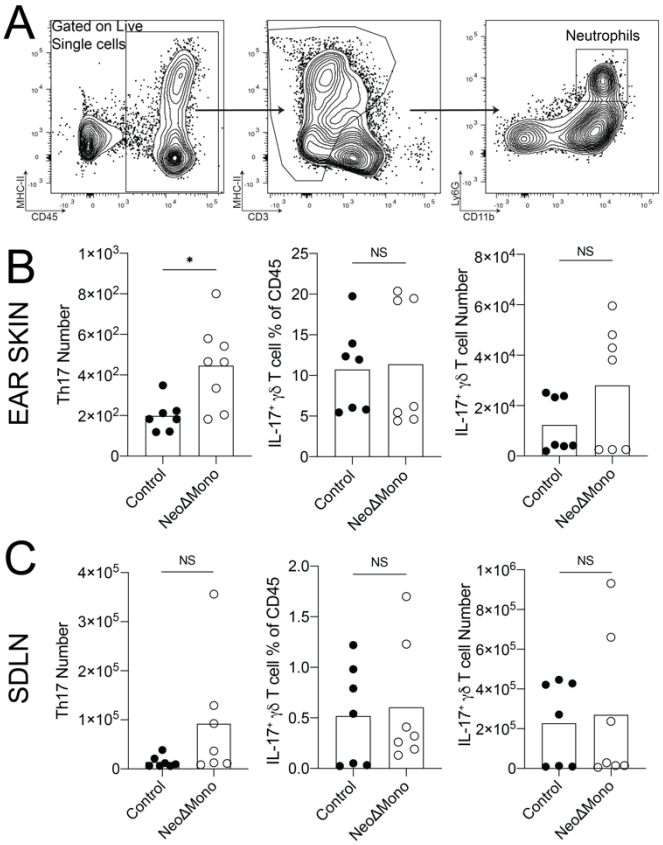

Figure S4: Related to main Figure 5
(A) Flow cytometric gating strategy to examine neutrophils in the skin and draining lymph nodes. (B-C) Quantification of IL-17A producing $CD4^+$ Teff cells and γδ T cells in the ear skin (B) and draining lymph nodes (SDLN) (C) of NeoΔmono and control mice treated with 5% imiquimod cream. Data in B-C is pooled data from two independent experiments. Statistical significance was determined using a two-tailed Student's t test where * is $p<0.05$.

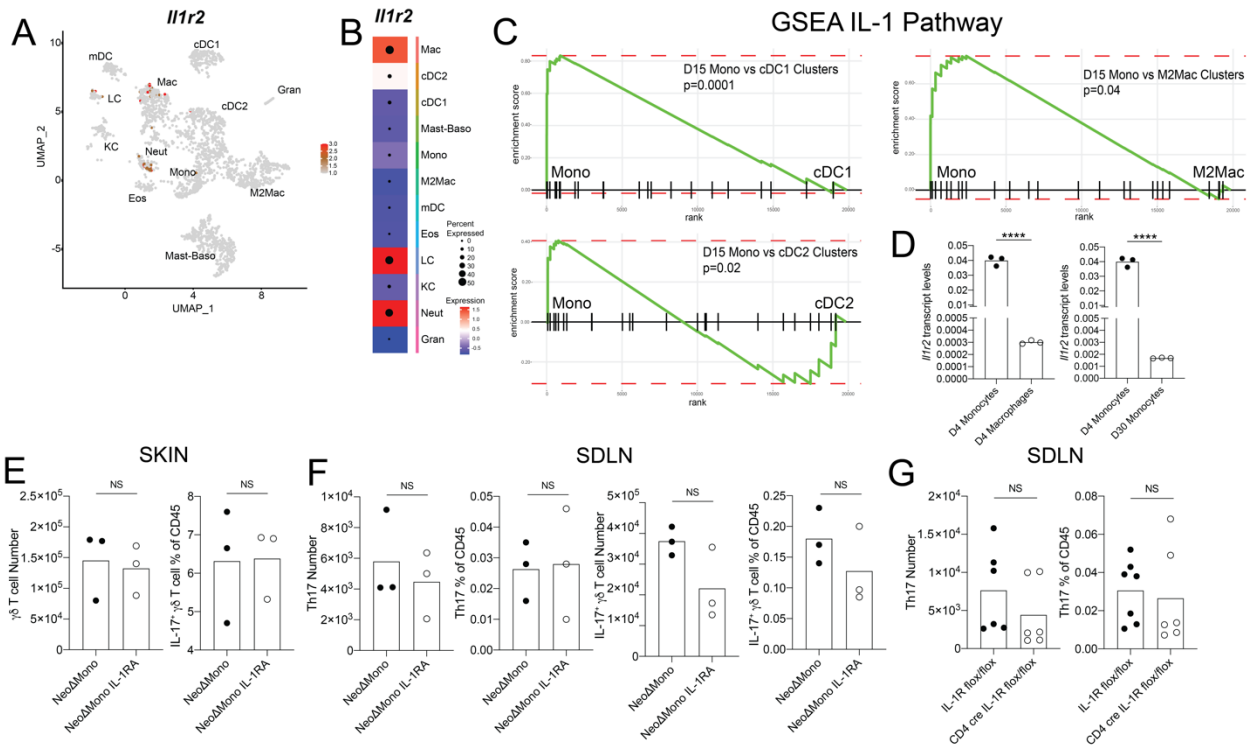

Figure S5: Related to main Figure 6 (A) UMAP from scRNA-seq analyses demonstrating expression levels of *Il1r2* on myeloid clusters in the skin of wild type postnatal Day 15 mice. (B) Heatmap quantification of normalized average expression (box color) and percentage of expressing cells (circle size) for *Il1r2* in individual myeloid clusters. (C) Gene Set Enrichment Analyses for IL-1 pathway genes comparing postnatal Day 15 skin monocyte and cDC1, M2Mac and cDC2 clusters. (D) qPCR analyses for *Il1r2* transcript levels comparing monocytes and macrophages from postnatal Day 4 skin and monocytes from postnatal Day 4 skin to monocytes from postnatal Day 30 skin. (E-G) Quantification of numbers of IL-17A producing γδ T cells in the skin (E) and SDLN (F) along with $CD4^+$ αβ T effector cells in the SDLN (F) of NeoΔmono mice treated with recombinant IL-1Ra or vehicle control. (G) Quantification of numbers of $CD4^+$ T effector cells producing IL-17A in the SDLN of *Cd4*^{cre}*Il1r1*$^{fl/fl}$ or control *Il1r1*$^{fl/fl}$ mice treated with anti-Gr-1 antibody in the neonatal window. Statistical significance was determined using a two-tailed Student's t test where * is p<0.05 and **** is p<0.0001. Data in E is one representative of three independent experiments and data in G is pooled from two experiments of at least three independent experiments.
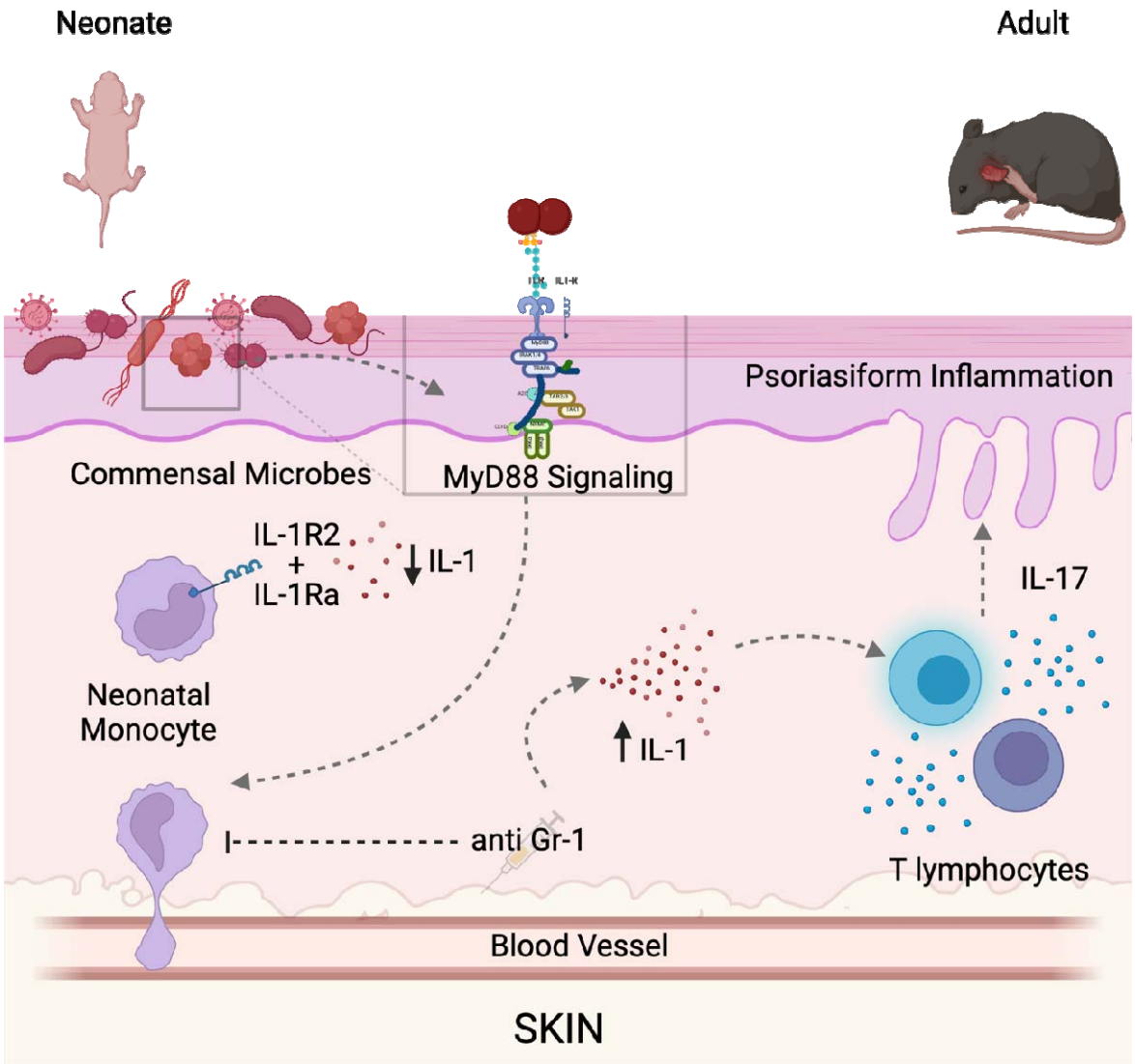
Commensal myeloid crosstalk in neonatal skin regulates long-term cutaneous type 17 inflammation